This manuscript was accepted and published by the ***Journal of Analytical and Applied Pyrolysis.***

Publication data of the final, corrected work:

Várhegyi, G.; Czégény, Zs.; Jakab, E.; McAdam, K.; Liu, C.: Tobacco pyrolysis. Kinetic evaluation of thermogravimetric – mass spectrometric experiments. *J. Anal. Appl. Pyrolysis* **2009**, *86*, 310-322. *doi:* 10.1016/j.jaap.2009.08.008

Tobacco pyrolysis. Kinetic evaluation of thermogravimetric – mass spectrometric experiments.

Gábor Várhegyi,[a,*] Zsuzsanna Czégény,[a] Emma Jakab,[a] Kevin McAdam[b] and Chuan Liu[b]

[a] *Institute of Materials and Environmental Chemistry, Chemical Research Center, Hungarian Academy of Sciences, P.O. Box 17, Budapest 1525, Hungary*

[b] *GR&D, British American Tobacco, Regents Park Road, Southampton SO15 8TL, United Kingdom*

[*] Corresponding author. Email: varhegyi.gabor@t-online.hu or gvarhegyi@gmail.com

Abstract

The thermal decomposition of two tobacco blends was studied by thermogravimetry - mass spectrometry (TGA-MS) at slow heating programs under well defined conditions. The kinetic evaluation was based on a distributed activation energy model (DAEM) which is a suitable tool for complex materials of plant origin. Linear and non-linear (stepwise) heating programs were employed to obtain information for reliable kinetic modeling. Series of experiments were evaluated simultaneously by the method of least squares. Efforts were made to identify and describe kinetically the similarities between two, highly different tobacco samples as well as between the various mass spectrometric intensity curves. This was achieved by evaluating large series of experimental results and assuming several kinetic parameters to be common for both samples and/or a group of mass spectrometric intensities.

The methods and considerations outlined in the paper may be helpful in the studies of biomass and other organic samples by a wider variety of experimental techniques including TGA-FTIR and time resolved pyrolysis.

Keywords: Tobacco; Thermal decomposition; Distributed activation energy model (DAEM);

Nomenclature

α_j	reacted fraction of a pseudocomponent
A_j	pre-exponential factor (s^{-1})
c_j	amount of volatiles formed from a unit mass of a pseudocomponent (See Eqs. (4) and (5))
$c_{normed,j}$	c_j coefficients normalized so that their sum equals to one (see Eq. (8))
$E_{0,j}$	mean activation energy in a distributed activation energy model (kJ mol^{-1})
FWHM	full width at half maximum (°C)
fit_N	a measure of the fit quality that expresses the difference between a group of N experimental curves and their simulated counterparts (%) (See Eqs. (5) and (6))
h_k	height of an experimental curve
$I(t)$	mass spectrometric intensity (in an instrument-specific, arbitrary unit)
$k(T)$	rate constant (s^{-1})
m	normalized sample mass (dimensionless)
$m^{calc}(t)$	normalized sample mass calculated from a model
$m^{obs}(t)$	mass of the sample divided by the initial sample mass
M	number of pseudocomponents
N	number of experimental curves in a least squares minimization or in the calculation of the fit quality
N_k	number of evaluated points on the kth experimental curve
$N_{parameters}$	number of unknown parameters in an evaluation
R	gas constant (8.3143×10^{-3} kJ mol^{-1} K^{-1})
σ_j	width parameter (variance) of Gaussian distribution
S_N	least squares sum formed from N experimental curves
τ	mean lifetime (s)
t	time (s)
T	temperature (°C, K)
X^{obs}, X^{calc}	experimental and simulated values of an evaluated quantity

Samples

B	Burley tobacco blend
V	Virginia tobacco blend

Subscripts:

i	digitized point on an experimental curve
j	pseudocomponent
k	experiment

1. Introduction

The primary goal of this work is to provide kinetic submodels for describing the pyrolysis of tobacco. In addition, we wish to introduce evaluation strategies that can be employed in the study of complex organic materials by evolved gas analysis or time-resolved pyrolysis techniques. The considerations, methods, and results of our work are thought to be useful for research on biomass and other organic materials, too.

Thermogravimetric measurements have a high precision while the temperature and the other experimental conditions of the sample are usually well known and well controlled. The coupling of a TGA with evolved gas analysis provides additional valuable information. This makes it a useful tool for studying devolatilization in the kinetic regime. On the other hand, TGA can be employed only at relatively low heating rates because the true temperature of the samples may become unknown at high heating rates.

Most materials of plant origin contain a wide variety of pyrolyzing species. Even the same chemical species may have differing reactivity if their pyrolysis is influenced by other species in their vicinity. The assumption of a distribution on the reactivity of the species frequently helps in the kinetic evaluation of the pyrolysis of complex organic samples [1]. The distributed reactivity is usually approximated by a Gaussian distribution of the activation energy, though other approaches are also available [1]. Distributed activation energy models (DAEM) have been used for biomass pyrolysis kinetics since 1985, when Avni et al. applied a DAEM for the formation of volatiles from lignin [2]. Later this type of research was extended to a wider range of biomasses and materials derived from plants, including several works on tobacco devolatilization [3-6] Saidi et al. employed DAEM-based kinetic models in establishing an actual combustion model of a burning cigarette [7].

Despite the complicated mathematics of this type of modeling, the works based on DAEM kinetics have frequently employed more than one parallel reaction. The resolution of the overlapping curves by parallel DAEM reactions and the finding of a good fit were achieved by a trial-and-error parameter-search in several works [8,9,3,10]. Burnham et al. reported a versatile, high-performance computer software in 1987 that was capable for the determination of the unknown model parameters by nonlinear regression [11]. The same software was also able to determine discrete, empirical distribution functions for the activation energy during the evaluation of non-isothermal experiments.

Holstein et al. [12] and de Jong et al. [10] reported a strong compensation effect between the parameters of the Gaussian DAEM. As de Jong et al. wrote [10]: "... it is more advantageous to fit A, E_0, and σ values to experimental data using a trial-and error approach. Non-unique solutions are usually found as a result of this fitting procedure, which is due to the so-called compensation effect. In other words, different pairs of kinetic parameters provide an equally good fit to experimental data. For this

reason, the values of pre-exponential factors are often fixed, and selected ... so that they are consistent with the transition-state theory ($A \approx 10^{11}$–10^{16} s^{-1})."

Várhegyi et al. [13] and Becidan et al. [14] based DAEM kinetic studies on the simultaneous evaluation of experiments with linear and stepwise temperature programs. This method served to increase the available experimental information, as outlined elsewhere [15]. The increase of the information content of the experiments is particularly important when overlapping processes are described by parallel DAEM reactions. The determination of the unknown model parameters and the verification of the model were based on the least-squares evaluation of series of experiments. This approach led to favorable results and allowed predictions outside the experimental conditions of the experiments used in the parameter determination [13,14]. This way was followed in the present work, too. A particular care was taken for employing a relatively low number of model parameters. This helped to achieve well-defined parameter estimation. Besides, efforts were made to express the similarities between the samples and the mass spectrometric intensity curves from detected volatiles during the modeling.

2. Experimental

2.1. Samples

Virginia and Burley tobaccos are the two tobacco varieties that are present in the largest quantities in most commercial tobacco products. Different growing and curing conditions have led to significant differences in their chemical compositions (Table 1). A Virginia and a Burley tobacco blend were thus investigated. The analysis of their constituents is summarized in Table 1. The main differences between the two tobacco samples are in the contents of the total sugars, total nitrogen and polyphenols. It may be interesting to note that these tobacco blends contain more minerals than a usual biomass fuel; the ash content of the Virginia and Burley blends were 12 and 20 %, respectively. The composition of the ash is similar in the two tobaccos, as shown by an ICP-AES spectrometry analysis in Table 2. Further characteristics of these samples can be found in an earlier work [16] that deals with pyrolysis – gas chromatography – mass spectrometry and thermogravimetry without a kinetic interpretation.

The tobacco samples for the experiments were taken from single-blend research cigarettes. The tobacco was slightly and gently broken to pieces of around 0.5 mm in an agate mortar for the experiments.

Table 1
Characteristics of the Virginia and Burley tobacco blends

m/m % on a dry weight basis	Virginia	Burley
Ash	11.9	20.3
Total nitrogen	2.7	4.7
Protein nitrogen	1.2	2.0
Ammonia nitrogen	0.0	0.5
Nitrate nitrogen	0.0	0.4
Total sugars	13.2	0.1
Nicotine	2.8	2.6
Cellulose	10.2	13.0
Lignin	3.7	4.2
Polyphenols (chlorogenic acid + rutin)	2.6	0.1

Table 2
Ash analysis[a]

m/m %	Virginia	Burley
Al	0.7	0.6
Ca	21.5	18.7
Fe	0.3	0.3
K	30.2	28.2
Mg	5.2	3.8
Na	0.4	0.4
P	2.0	1.4
S	2.1	1.7
Si	1.6	1.5
Sr	0.1	0.1

[a] The ash was prepared by CEN/TS 14775 standard. The analysis was carried out on 19 elements of which the concentration of As, Ba, Cr, Cu, Mn, Mo, Ni, Pb, and Zn was below 0.05%.

2.2. TGA-MS experiments

TGA – MS experiments were performed by a computerized Perkin-Elmer TGS-2 thermobalance connected to a Hiden HAL quadrupole mass spectrometer. The measurements were carried out using argon purge gas with a flow rate of 140 ml min^{-1}. Each experiment started with a 45-min purge at room temperature to flush out the trace oxygen from the system. A portion of the volatile products was introduced to the mass spectrometer through a heated capillary transfer line. The mass spectrometer was operated in electron impact ionization mode with 70 eV electron energy. The unit of the normalized mass spectrometric intensities was regarded as an arbitrary unit specific to the given apparatus. Accordingly, the term "arbitrary unit" was used in the figures and tables, similarly to the other works with this instrument and its predecessors since the paper of Blazsó et al. in 1985 [17].

As outlined earlier [15], the inclusion of stepwise temperature programs into the series of experiments increases the information content for the kinetic evaluation. Accordingly, three linear and two stepwise programs were employed, as shown in Fig. 1. Heating programs □ □ □, ○ ○ ○, •••• and —— were also used in a combustion study by TGA which will be published elsewhere. The differences of heating programs •••• and —— reflect reactivity differences between the Virginia and the Burley samples. The highest isothermal sections in these programs, 410 and 415°C, respectively, are the highest isothermal temperatures at which combustion studies can be carried out in our instrument without the ignition of these samples. In the present work the sample mass was around 1 mg at 40°C/min and 4 mg in the other cases. The samples were evenly distributed on a platinum sample pan of 6 mm diameter. The relatively low sample masses served to avoid the self-cooling of the samples due to the endothermic reaction heat.

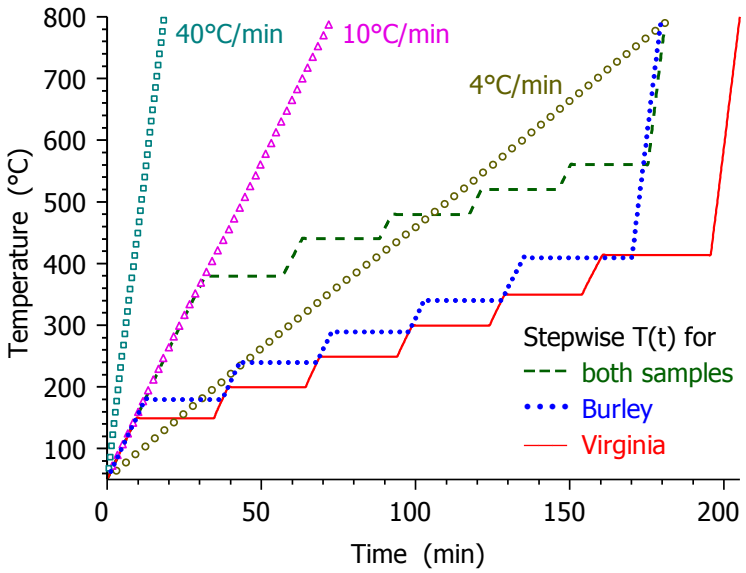

Fig. 1. The temperature programs of the experiments.

Around 100 mass spectrometric intensities were measured in two test experiments. An initial survey of these data revealed that eleven mass spectrometric intensities had sufficiently good signal/noise and signal/background ratios for the kinetic evaluation. They are shown in Table 3. A low concentration isotope of the carrier gas, ^{38}Ar was also measured as an internal sensitivity calibration, as described in the next paragraph. The level of the trace oxygen (m/z 32) was recorded to check the hermetic closure of the system. In this way the rest of the TGA-MS experiments were carried out with 13 intensities, which permitted longer scanning time (lower noise) and shorter overall time.

Table 3.
Mass spectrometric intensities selected for kinetic evaluation

Mass/charge	formula and possible sources
m/z 2	H_2
m/z 15	CH_3^+ (mainly methane)
m/z 18	H_2O
m/z 27	$C_2H_3^+$ (+ HCN)
m/z 28	mainly CO
m/z 29	CHO^+, $C_2H_5^+$
m/z 30	$HCHO^+$ (+ CH_3NH^+, NO^+)
m/z 31	CH_3O^+ (e.g. from methanol)
m/z 41	$C_3H_5^+$, (C_2HO^+)
m/z 43	CH_3CO^+, $C_3H_7^+$
m/z 44	CO_2

2.3. Baseline corrections and scale factors

Each experimental curve was normalized by the sample mass after drying. For this purpose the TGA value at 120°C was used. The ion intensities were also normalized by the intensity of the ^{38}Ar isotope in the carrier gas, as an internal calibration of the instrument sensitivity. Ion *m/z* 28 was corrected by subtracting the intensity of corresponding fragment ion of carbon dioxide. It is well known that mass spectrometers have background values that may change with time. As a correction, approximate linear baselines were formed by selecting a low and a high temperature value on each curve where the production of the corresponding volatiles was assumed negligible. In the case of hydrogen the baselines were horizontal because the hydrogen formation could not be assumed to be negligible at any high temperature in the domain of the investigations.

A particular problem in the kinetic evaluation of the mass spectrometric data is a moderate variation of the instrument sensitivity with time and experimental conditions. The results of the TGA-MS experiments depend on the combined sensitivity of the various parts of the instrument, including (i) the dilution of the products in the carrier gas in the TGA furnace; (ii) the transfer from the furnace to the MS ion source; (iii) and the sensitivity of the mass spectrometer itself. To deal with these aspects, each simulated kinetic curve was multiplied by a scale factor that expressed the instrument sensitivity for the given mass spectrometric ion in the given experiment. As mentioned above, each mass spectrometric intensity curve was available at different experiments. In each group of five experiments the mass spectrometric intensity of the 40°C/min experiment was used as a reference point (its scale factors were set to unity). The unknown scale factors were determined in the least squares kinetic evaluation together with the model parameters, as described later in the text. In this way the scale factors measured the sensitivity changes in comparison to the corresponding 40°C/min experiment. It turned out during the

evaluations that the slower experiments needed usually higher scale factors than the 40°C/min experiments: the mean of the scale factors without the 40°C/min experiments was 1.2. This effect indicates that the heating rate probably had some influence on the dilution of the products by the carrier gas in the TGA furnace.

3. Model and methods

3.1. Distributed activation energy model (DAEM)

As mentioned in the *Introduction,* a model of parallel reactions with Gaussian activation energy distribution was chosen due to the favorable experience with this type of modeling on similarly complex materials [13,14]. According to this model the sample is regarded as a sum of M pseudocomponents. Here a pseudocomponent is the totality of those decomposing species which can be described by the same reaction kinetic parameters in the given model. In the present work 1 – 4 pseudocomponents will be employed. The number of reacting species is obviously much higher in a complicated mixture of plant materials. The reactivity differences are described by different activation energy values. On a molecular level each species in pseudocomponent j is assumed to undergo a first-order decay. The corresponding rate constant (k) and mean lifetime (τ) are supposed to depend on the temperature by an Arrhenius formula:

$$k(T) = \tau^{-1} = A_j \, e^{-E/RT} \qquad (1)$$

Let $\alpha_j(t,E)$ be the solution of the corresponding first order kinetic equation at a given E and $T(t)$ with conditions $\alpha_j(0,E)=0$ and $\alpha_j(\infty,E)=1$:

$$d\alpha_j(t,E)/dt = A_j \, e^{-E/RT} [1-\alpha_j(t,E)] \qquad (2)$$

The density function of the species differing by E within a given pseudocomponent is denoted by $D_j(E)$. $D_j(E)$ is approximated by a Gaussian distribution with mean $E_{0,j}$ and width-parameter (variation) σ_j. The overall reacted fraction of the jth pseudocomponent, $\alpha_j(t)$ is obtained by integration:

$$\alpha_j(t) = \int_0^\infty D_j(E) \; \alpha_j(t,E) \, dE \qquad (3)$$

The normalized sample mass, m, and its derivative are the linear combinations of $\alpha_j(t)$ and $d\alpha_j/dt$, respectively:

$$-dm/dt = \sum_{j=1}^{M} c_j \, d\alpha_j / dt \quad \text{and} \quad m(t) = 1 - \sum_{j=1}^{M} c_j \alpha_j(t) \qquad (4)$$

where a weight factor c_j is equal to the amount of volatiles formed from a unit mass of pseudocomponent *j*. c_j is dimensionless in Eq. (4). When mass spectrometric intensity curves are evaluated, the calculated intensity curves, *I(t)* are obtained as a linear combination of $d\alpha_j/dt$:

$$I(t) = scalefactor \sum_{j=1}^{M} c_j d\alpha_j / dt \qquad (5)$$

where *scalefactor* is the sensitivity factor introduced in Section 2.3. As mentioned in the Experimental section, the mass spectrometric intensities are in an arbitrary unit accordingly the dimension of c_j in Eq. (5) is also an arbitrary unit.

3.2. Evaluation by the method of least squares

The unknown model parameters and the scale factors described in Section 2.3 were evaluated from series of experiments by minimizing sum S_N:

$$S_N = \sum_{k=1}^{N} \sum_{i=1}^{N_k} \frac{\left[X_k^{obs}(t_i) - X_k^{calc}(t_i)\right]^2}{N_k h_k^{\,2}} \qquad (6)$$

Here *N* is the number of the experimental curves in the given evaluation. In the present work its value varied between 5 and 50. Subscript *k* indicates the different experiments. X_k^{obs} and X_k^{calc} denote the observations and their simulated counterparts. t_i denotes the time values in which the discrete experimental values were taken, and N_k is the number of the t_i points in a given experiment. h_k denotes the heights of the experimental curves that strongly depend on the experimental conditions. The division by h_k^2 serves for normalization. The fit is characterized by a measure of the difference between the experimental curves and their simulated counterparts:

$$fit_N\,(\%) = 100\ S_N^{0.5} \qquad (7)$$

Equations (6) and (7) can be employed to express the quality of the fit of any group of evaluated experiments. When the fit is calculated for one experiment, fit_1 equals to the root mean square (rms) deviation expressed as the percent of peak maximum.

3.3. Numerical methods

Fortran 95 and C++ programs were employed that were developed and tested on various biomass materials by one of the authors [13-15,18,19]. Here we give a brief description of the algorithms employed and some essential details that were omitted in our earlier works. The derivatives of the sample mass curves (DTG) were determined by the analytical differentiation of smoothing splines, as described by Várhegyi and Till [20]. The rms difference between the spline function and the measured TGA data was between 0.1 and 0.4 μg. This procedure does not introduce considerable systematic errors into the least squares kinetic evaluation of series of experiments [19]. The kinetic equations of the model were

solved numerically along the empirical temperature – time functions resulting in simulated data in the t_i points of the observations. The integration by E in the DAEM kinetics was carried out by a Gauss – Hermite quadrature formula, as described by Donskoi and McElwain [21] and Várhegyi et al. [13]. The domain of integration was rescaled by a factor of 0.2 to increase the precision of the integration [13,21]. The first order kinetic equations of the DAEM were solved numerically in 180 quadrature points. Obviously the solution of the kinetic equations is not needed in the lower and higher ends of the activation energy range. This can be easily checked by Eq. (1): if the mean lifetime is lower than 10^{-3} s in the first evaluated point of the domain of evaluation, then the corresponding species surely decompose before reaching the domain of evaluation. (The actual limit should obviously be set to the time scale and precision requirements of the given work. A limit can also be implemented in the solution of the first order kinetic equations: the integration can obviously be finished if the normalized amount of the given species reaches a low value, e.g. 10^{-12}.) A similar limit can also be set at the high end of the E domain by calculating the mean lifetime at the highest evaluated temperature. If it is much higher than the time scale of the problem then only a negligible part of the corresponding species will decompose and the kinetic equation need not be solved at this E.

After separating the variables in the first order kinetic equations, the exponential integral was solved numerically in each $[t_{i-1},t_i]$ interval by a Gauss – Legendre quadrature of 7 points of which the first and last ones were fixed to be at the end points of the given $[t_{i-1},t_i]$ interval [22]. This procedure works at any $T(t)$ function that may arise in thermal analysis. A linear T(t) was assumed at the beginning of the integration, from room temperature to the first point of the evaluation, accordingly it is possible to use an analytic approximation of the exponential integral in this interval. Legendre's continued fractions were employed there [23]. The minimization by the linear parameters of the model, (c_j) is equivalent to the solution of a system of linear equations that easily can be carried out at each set of non-linear parameters [18]. The minimization of the least squares sum by the non-linear parameters was carried out by a variant of the Hook–Jeeves method, which is a slow but simple and reliable direct search algorithm [24]. In our work the original Hook–Jeeves algorithm was supplemented by a parabolic interpolation to find optimal step sizes in each search direction. The starting values for the non-linear optimization were taken either from earlier work [13,19] or from the results of the simpler evaluations of the present work.

The calculations were carried out on personal computers under Microsoft Windows®. The average solution time of a DAEM equation was around 25 ms on an Intel® Core™ 2 Quad Q9550 processor running at 2.8 GHz. (The parallel processing capabilities of this processor were not used in our work. The utilization of all processor cores could obviously multiply the speed of this type of calculations.). The simulation of 50 curves at two partial DAEM reactions required around 2.5 s. The time of a least squares evaluation varied between 5 minutes and 10 hours depending on the number of curves evaluated simultaneously, the number of the unknown parameters and the distance of the solution from the initial

parameters. The above information is provided to orient the readers about the applicability of the results as kinetic submodels for larger modeling works.

3.4. Notes on the figures of this work

This work is based on the reaction kinetic evaluation of 10 DTG curves and 110 MS intensity curves. Each of these curves was used in several evaluations. Obviously only a subset of the results can be presented as figures. One occurrence of each 10°C/min experimental curve will be shown in the figures on the kinetic evaluation. The full version of the figures with all experimental curves is available as *Supplementary Content* alongside with the electronic version of this publication at http://www.sciencedirect.com/.

4. Results and Discussion

4.1. Evaluation of the DTG curves

In the first step of the work the two samples were evaluated separately. N was 5 in the least squares sum (Eq. (6)). The calculations were started by the assumption of one DAEM reaction (M=1 in Eq. (4)). In this case the overall fit quality calculated on both samples (fit_{10}) was ca. 8%. fit_{10} gradually improved as M increased. The change from M=3 to M=4 resulted in a particularly high improvement: fit_{10} decreased from 4% to 2%. Accordingly the evaluation at M=4 was selected for a closer view. The corresponding parameters can be found in the first and second columns of Table 4, under heading "Evaluation 1". The first row in the table body shows the parameters that are assumed to have common values for the two samples; it is "none" in the present case. The last row of the Table shows how many unknown parameters were determined from one experiment ($N_{parameters}/N$). In Evaluation 1 the parameters showed large differences between the two samples. One can expect the pyrolysis kinetics of the tobaccos to show some similarities because they contain essentially the same plant components (Table 1). The differences between the devolatilization of the different tobacco blends may be due to the different amounts of the components, to minor differences in the chemical structure of the components and to possible catalytic effects of the mineral content on the decomposition reactions [25,26]. The assumption of common parameters for the different samples is a straightforward way to express similarities [19]. Besides, this approach makes the parameter estimation mathematically better defined by decreasing the number of the unknown parameters, as shown by $N_{parameters}/N$.

Table 4
Evaluation of the DTG curves with different assumptions on the kinetic parameters

Evaluation	**1**		**2**		**3**		**4**		**5**	
Sample	V	B	V	B	V	B	V	B	V	B
Common parameters	none		$E_{0,j}$		$E_{0,j}$ and σ_j		$E_{0,j}$ and A_j		$E_{0,j}$, σ_j, and A_j	
fit_{10} / %	2.0		2.1		2.4		2.7		2.9	
$E_{0,1}$ / kJ mol^{-1}	119	208	123		118		122		116	
$E_{0,2}$ / kJ mol^{-1}	209	227	201		202		195		196	
$E_{0,3}$ / kJ mol^{-1}	201	215	206		205		203		203	
$E_{0,4}$ / kJ mol^{-1}	239	308	254		252		259		251	
σ_1 / kJ mol^{-1}	7.7	29.5	8.1	9.6	9.9		10.1	6.7	8.1	
σ_2 / kJ mol^{-1}	10.7	1.4	10.7	1.9	4.9		5.6	7.6	7.3	
σ_3 / kJ mol^{-1}	3.1	3.6	3.4	5.6	4.7		6.2	4.7	4.8	
σ_4 / kJ mol^{-1}	37.9	18.0	37.1	39.0	40.2		34.4	36.3	38.6	
$\log_{10} A_1$ / s^{-1}	11.51	16.75	11.93	10.83	11.11	10.47	11.58		10.96	
$\log_{10} A_2$ / s^{-1}	17.99	20.05	17.22	17.54	17.40	17.60	16.91		16.88	
$\log_{10} A_3$ / s^{-1}	15.48	17.05	15.90	16.29	15.93	16.13	15.87		15.79	
$\log_{10} A_4$ / s^{-1}	17.61	19.69	18.59	18.60	18.77	18.59	18.61		18.39	
c_1	0.11	0.43	0.12	0.08	0.14	0.06	0.17	0.05	0.13	0.05
c_2	0.11	0.03	0.13	0.05	0.06	0.07	0.07	0.13	0.08	0.11
c_3	0.08	0.07	0.08	0.13	0.10	0.12	0.13	0.12	0.11	0.11
c_4	0.38	0.08	0.35	0.36	0.38	0.38	0.31	0.32	0.36	0.35
$N_{parameters}$/N	3.2		2.8		2.4		2.4		2.0	

The assumption of common $E_{0,j}$ values practically did not effect fit_{10} and reduced the number of the strongly different parameters to one: only σ_2 showed high differences between the two samples in Evaluation 2. The assumption of common $E_{0,j}$ and σ_j further increased the similarities. At linear heating programs the widths of the partial curves (FWHM) are nearly the same in the two samples at this evaluation, as Fig. 2 shows, while the peak temperatures and peak heights show some variation. Note that the T_{peak} and FWHM values are indicated in Fig. 2. At nearly identical FWHM values the height of the curves is defined mainly by the c_j parameters that can be found in Table 4.

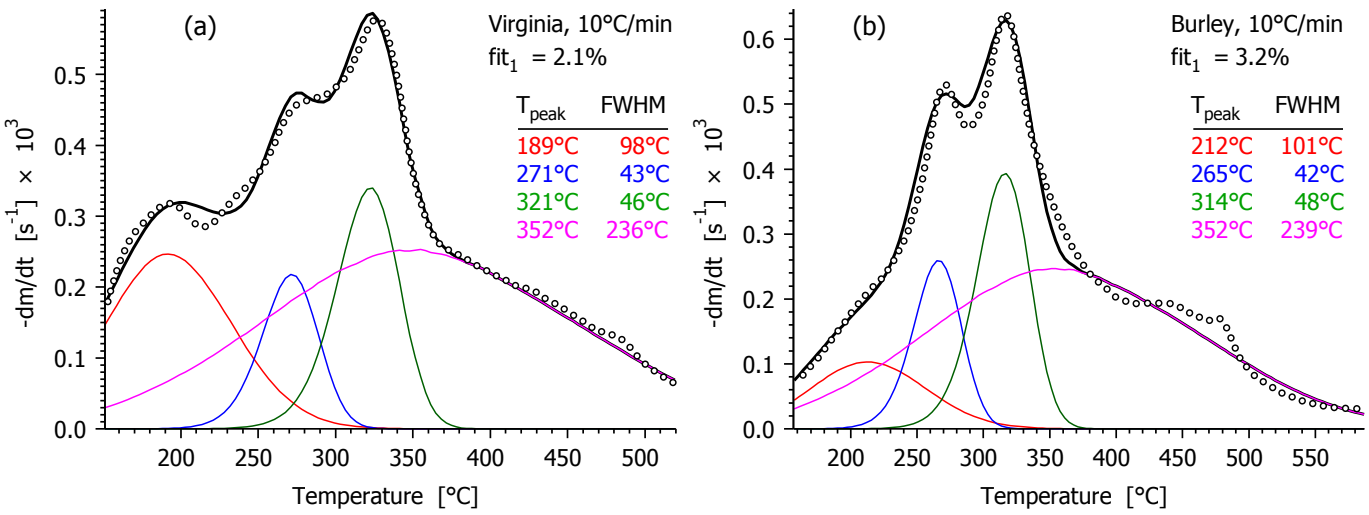

Fig. 2. Evaluation of ten DTG curves assuming identical $E_{0,j}$ and σ_j parameters for both samples. The experimental data (∘∘∘), their simulated counterparts (—) and the calculated partial curves (—) are shown for the 10°C/min experiments. See Evaluation 3 in Table 4 for the corresponding parameters.

The assumption of common $E_{0,j}$ and A_j values diminish the peak temperature differences between the samples, as the results of the next section illustrate, while common $E_{0,j}$, σ_j, and A_j values reduce the variation of both the peak temperatures and the peak widths. It is interesting to note that the $E_{0,j}$ parameters have practically the same values in Evaluations 2 – 5.

Unfortunately the statistical significance of the changes in the fit_{10} values cannot be determined because the main experimental errors of the thermal analysis are neither random nor independent [15]. However, the differences in the fit quality do not appear to be dramatic from a practical point of view. The approaches shown here are different approximations (different ways of approximate modeling) of the same physical reality. Figure 2 (Evaluation 3) corresponds to the middle of the fit_{10} range of Table 4.

The chemical identification of the calculated peaks is difficult because the samples consist of many components. The first peak covers obviously the low temperature processes, including the thermal decomposition of sugars and pectins and the evaporation of some species that are volatile in this domain [27,28]. The shape and position of the second and third peaks are similar to the partial curves of hemicelluloses and celluloses in biomass materials [26,28,29]. The fourth, very wide peak incorporates the many minor components of the tobacco blends of which the thermal decomposition merges into a wide distribution. As Table 1 shows, the samples contain around 4% lignin that also decomposes in a wide temperature domain [30]. At the higher end of the temperature domain this peak covers the slow char forming reactions [28].

4.2. Common evaluation of five mass spectrometric intensities that showed similar behavior

As outlined in the Experimental section, the mass spectrometric intensity curves involve more experimental uncertainties than the DTG curves. Accordingly one cannot expect as good fit values as in

the case of the DTG curves. We shall deal only with the main features of these curves and disregard their finer details. Besides, a larger number of experimental curves will be evaluated together so that their uncertainties could be averaged out in the least squares curve fitting. Test evaluations were carried out to find a group for a joint evaluation with several common parameters. Five mass spectrometric intensities proved to be similar in this respect:

m/z 15 CH_3^+ (mainly methane)

m/z 29 CHO^+, $C_2H_5^+$

m/z 30 $HCHO^+$ (+ CH_3NH^+, NO^+)

m/z 43 CH_3CO^+, $C_3H_7^+$

m/z 44 CO_2

They were described by two parallel reactions because they evidenced two main peaks. Note that the CO_2 evolution showed a third peak with T_{peak} above 600°C that was particularly marked in the Burley sample. This peak was due to the decomposition of mineral carbonates and was not investigated: the intensity curves at m/z 44 were truncated at the start of the third peak. The rest of the chemical reactions in this group were due mainly to the primary decomposition of the various carbohydrates below 400°C and to the formation of the charcoal structure above 400°C, as outlined in the next section.

Similar strategies were employed as in the previous section. In the present case, however, three different possibilities were considered for the scope of a parameter value:

(i) same for all experimental conditions, different at different intensity curves and samples;

(ii) same for both samples at all experimental conditions, different at different intensity curves;

(iii) same for the five mass spectrometric fragments at both samples and at all experimental conditions.

Table 5 contains the results at various assumptions on the parameters.

As in the case of the DTG evaluation, the assumption of common $E_{0,j}$ values (Evaluation II) hardly changed the fit quality, while $N_{parameters}/N$ decreased from 2.4 to 2.0. As discussed in Section 2.3, the changes in the instrument sensitivity were described by scale factors which added 0.8 to $N_{parameters}/N$. (4 scale factors for each group of 5 experimental curves). The $N_{parameters}/N$ values of Table 5 include this term. The c_j parameters were normalized for comparable heights before averaging them for Table 5 due to the high differences in their magnitudes:

$$c_{normed,j} = c_j / (c_1+c_2), \quad j=1, 2 \qquad (8)$$

From Evaluation I to VI the quality of the fit gradually worsened. There was a higher increase in fit_{50} from Evaluation VI to VII because the assumption of common $E_{0,j}$ and A_j values forced the peak temperature of the intensity curves close to each other. In the case of evaluation VIII all kinetic parameters ($E_{0,j}$, A_j and σ_j) were assumed to be common for the five m/z values and only c_j was allowed to vary with m/z and tobacco properties. In this approximation the shape and position of the partial peaks

are exactly identical in all the 50 experimental curves. Though the fit was rougher in this way (fit_{50}=10%), the common handling of a variety of volatiles may be advantageous in combustion models due to the higher computational speed and the lower number of parameters.

Table 5 displays the mean values in angular brackets of those parameters that varied in the given evaluation. It is interesting to note that the parameters listed in Table 5 show only small variations in Evaluations I – VIII. One can conclude that 50 experimental curves together reasonably define these values. The similarity between the reactions producing the different intensities is expressed by the parameters listed in the first row. As the results of Evaluation VI show, one can assume common $E_{0,1}$, $E_{0,2}$, σ_1 and σ_2 values for the five intensities without a dramatic change in the fit quality.

The parameters indicated in the second row of Table 5 express the similarity between the samples in the given evaluation. When σ_1 and σ_2 were assumed to be independent from the tobacco sample in Evaluation IV, the widths of the partial curves of a given intensity were nearly identical for the two samples. However, better fit quality was obtained when A_1 and A_2 were assumed to be independent from the tobacco sample (Evaluation III in Table 5). The corresponding parameters are listed in Table 6 together with the calculated peak maxima ($T_{peak,j}$) and peak widths ($FWHM_j$) values at 10°C/min. Due to the common A and E values, the $T_{peak,j}$ values are nearly the same for the two tobacco blends in this evaluation. Fig. 3 displays the 10°C/min experiments of Evaluation III.

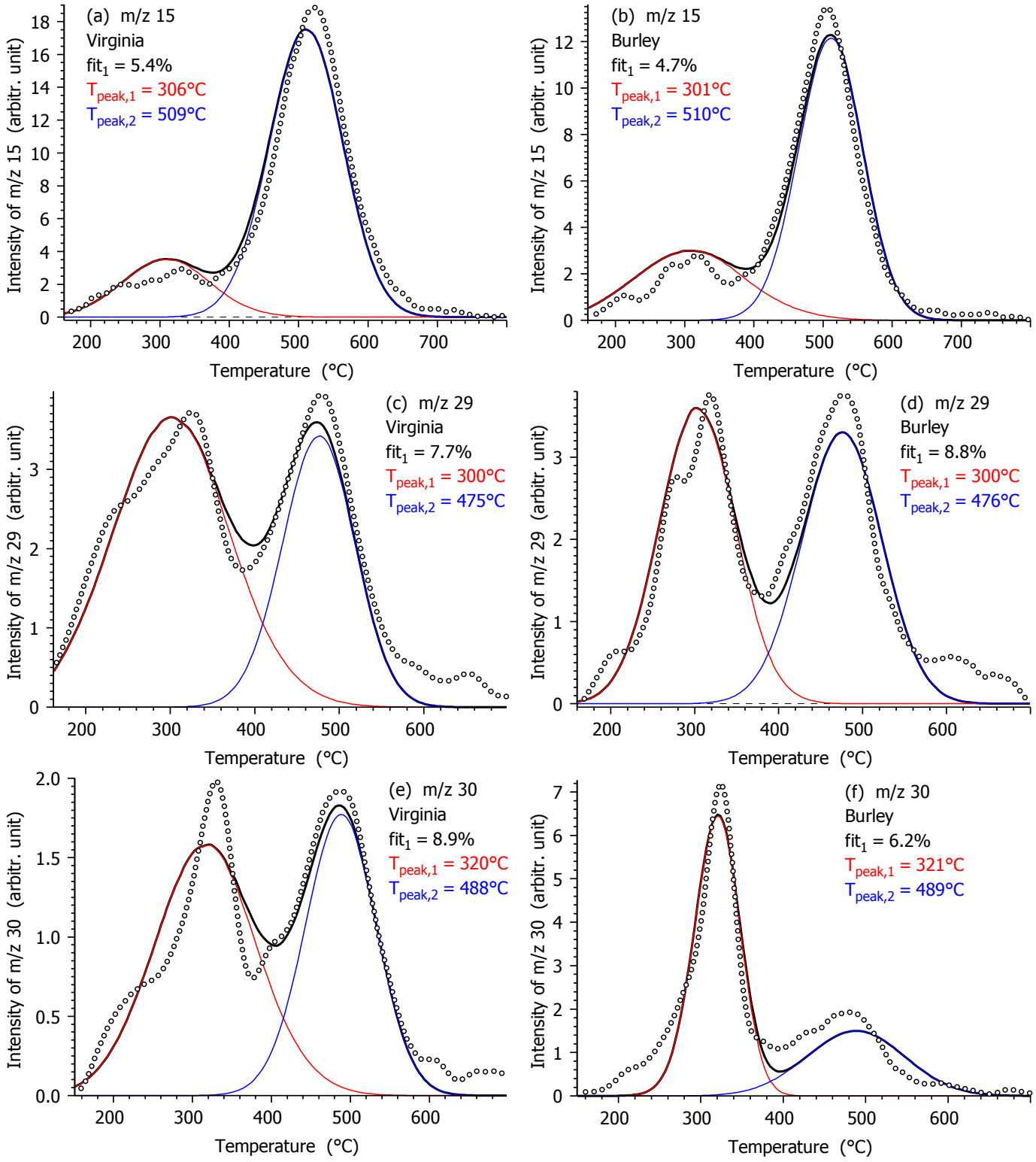

Fig. 3. Simultaneous evaluation of fifty MS intensity curves as described in Section 4.2. The experimental data (∘∘∘), their simulated counterparts (—) and the calculated partial curves (—) are shown for the 10°C/min experiments. The corresponding parameters are listed in Table 6.

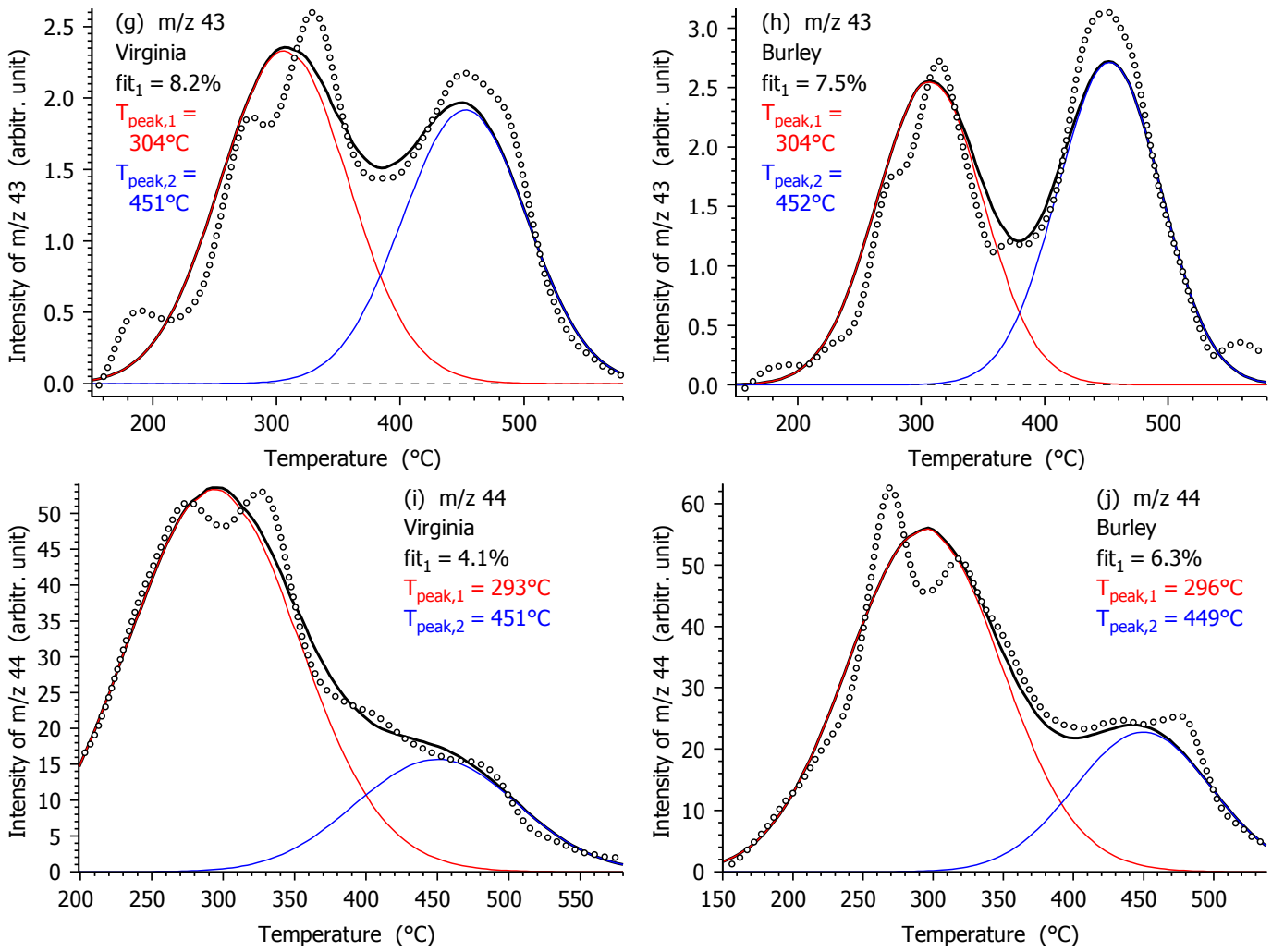

Fig. 3. *(Continued.)*

Table 5
Evaluation of five intensities (50 experimental curves) together with different assumptions on the parameters, as described in the text. (Brackets < > indicate average values.)

Evaluation	**I**	**II**	**III**	**IV**	**V**	**VI**	**VII**	**VIII**
Parameters with scope (iii)	–	$E_{0,j}$	$E_{0,j}$	$E_{0,j}$	$E_{0,j}$	$E_{0,j}$, σ_j	$E_{0,j}$, A_j	$E_{0,j}$, A_j, σ_j
Parameters with scope (ii)	–	–	A_j	σ_j	A_j, σ_j	A_j	σ_j	–
Parameters with scope (i)	$E_{0,j}$, A_j, σ_j, c_j	A_j, σ_j, c_j	σ_j, c_j	A_j, c_j	c_j	c_j	c_j	c_j
fit_{50} / %	5.7	5.8	6.2	6.7	6.9	7.2	9.9	10.3
$E_{0,1}$ / kJ mol^{-1}	<225>	211	211	210	210	214	224	226
$E_{0,2}$ / kJ mol^{-1}	<273>	262	266	262	262	263	280	280
σ_1 / kJ mol^{-1}	<21.8>	<20.3>	<20.1>	<20.1>	<20.3>	20.4	<21.3>	24.8
σ_2 / kJ mol^{-1}	<16.2>	<15.4>	<15.9>	<15.0>	<15.0>	14.5	<16.8>	17.6
$\log_{10} A_1$ / s^{-1}	<18.2>	<16.9>	<16.9>	<16.8>	<16.8>	<17.1>	17.9	18.1
$\log_{10} A_2$ / s^{-1}	<17.0>	<16.2>	<16.4>	<16.1>	<16.1>	<16.1>	17.2	17.1
$c_{normed,1}$	<0.54>	<0.54>	<0.54>	<0.54>	<0.55>	<0.55>	<0.56>	<0.58>
$c_{normed,2}$	<0.46>	<0.46>	<0.46>	<0.46>	<0.45>	<0.45>	<0.44>	<0.42>
$N_{parameters}/N$	2.4	2.0	1.8	1.8	1.6	1.5	1.5	1.3

Table 6
Parameters and peak characteristics obtained by Evaluation III of Table 5.[a]

MS ion	m/z 15		m/z 29		m/z 30		m/z 43		m/z 44	
Sample	V	B	V	B	V	B	V	B	V	B
fit_{10}	4.8		7.0		6.9		7.0		4.8	
$\log_{10} A_1$	16.78		17.03		16.52		16.89		17.34	
$\log_{10} A_2$	15.47		16.33		16.03		16.95		17.02	
σ_1	22.8	29.4	25.5	16.1	23.1	8.3	18.6	15.0	22.2	20.1
σ_2	16.5	14.1	13.5	15.3	14.0	19.6	16.8	13.5	19.3	16.3
$c_1 / 10^3$	2.5	3.0	2.8	1.9	1.2	2.2	1.6	1.4	40.3	37.3
$c_2 / 10^3$	10.2	7.0	1.7	1.9	0.9	1.1	1.3	1.5	11.6	14.0
Characteristics of the calculated peaks at 10°C/min:										
$T_{peak,1}$	306	301	300	300	320	321	304	304	293	296
$T_{peak,2}$	509	510	475	476	488	489	451	452	451	449
$FWHM_1$	149	188	164	107	152	65	122	101	141	131
$FWHM_2$	125	110	99	111	106	139	117	99	131	115

[a] Five intensities (50 experimental curves) were evaluated simultaneously. $E_{0,1}$ and $E_{0,2}$ were 211 and 266 kJ mol^{-1}, respectively, as indicated in Table 5. c_1 and c_2 are in an arbitrary unit.

4.3. The chemistry behind the mass spectrometric intensities evaluated together

The chemical interpretation of the above treated mass spectrometric intensities can be based on earlier TGA-MS work on biomasses and other plant materials [26,30-32]. With the exception of m/z 27, the mass spectrometric intensities in this group were described by a low temperature peak around 300°C and a high temperature peak around 450 – 500 °C. The low temperature peak can be due mainly to the thermal decomposition of cellulose and hemicellulose while the higher temperature peak can be associated with the gradual formation of the charcoal structure. The lignin content of the samples contributes volatiles in the whole domain of evaluation [30]. In the following section the intensity curves of this group will be listed and commented one by one.

(a) **m/z 15.** This mass/charge ratio corresponds to fragment ion CH_3^+. It forms mainly from methane, but almost all organic compounds containing $–CH_3$ groups can produce small amounts of CH_3^+. Its intensity exhibited a small, wide peak at low temperature and a much higher peak at higher temperatures. The low temperature peak arises from a variety of compounds containing $-CH_3$ groups, while the higher temperature peak is methane. This was verified by comparing intensities m/z 15, 16 and 17 in test experiments. The comparison of m/z 15 and m/z 16 showed that the methane formation from the Virginia sample is negligible below 300°C. In the case of the Burley sample a significant ammonia production was observed that dominated the low temperature parts of the ions at m/z 16. (The kinetics of the ammonia production was not studied in the present work. Intensities m/z 16 and 17 were corrected in these tests by the corresponding fragment ions of the main decomposition products, H_2O, CO and CO_2, respectively.)

(b) **m/z 29** corresponds mainly to ions CHO^+ and $C_2H_5^+$. The first is characteristic to aldehydes. This is the most abundant fragment of formaldehyde, but other organic compounds can also produce it. $C_2H_5^+$ is a low-abundance fragment of several compounds containing $-C_2H_5$. Ion CHO^+ from formaldehyde and other aldehydes dominates this intensity in the slow pyrolysis of biomass and tobacco.

(c) **m/z 30** corresponds mainly to fragment ion $HCHO^+$. This is the molecular ion of formaldehyde. The Burley sample contained 0.4% nitrate nitrogen (See Table 1). The nitrogen oxides produced from the nitrates also appear at m/z 30 as NO^+ ions. As the comparisons of plots (e) and (f) in Fig. 3 shows, the low temperature peak is much higher at the Burley sample, while the second peaks have comparable magnitudes. (On the experimental curves the height of the second peak is around 2 units, while the first peak has heights of 2 and 7 units in plots (g) and (h), respectively.)

(d) **m/z 43** corresponds mainly to fragment ion CH_3CO^+ that forms mostly from compounds containing CH_3-CO- and $-CH_2$-CO- structures [33]. $C_3H_7^+$, forming from aliphatic hydrocarbons, also appears here. As plots (i) and (j) show in Fig. 3, several "shoulders" appear on these curves that were approximated by two peaks in the present model.

(e) **m/z 44** belongs to CO_2. The low temperature sections of its intensity curve can be due to the thermal decomposition of carboxylic groups (organic acids and their salts). Note that the Virginia sample evidenced a side peak below 200°C that was not evaluated. The high temperature decomposition of the mineral carbonates was also excluded from the kinetics, as mentioned earlier. High CO_2 evolution was observed from ca. 200 to ca. 500-600°C in biomasses and cellulose [26,31,32]. Lignins release significant amount of CO_2 from ca. 200°C till temperatures above 600°C [30].

4.4. Evaluation of intensities m/z 27 and m/z 41

Both m/z 27 and m/z 41 arise mainly from C_2 compounds. m/z 27 mostly consists of $C_2H_3^+$ ions that form from many compounds containing aliphatic C-C groups. The small amount of HCN reported in pyrolysis tobacco studies [3-6] also appears at m/z 27. m/z 41 has two sources. Fragment ion C_2HO^+ forms mainly from compounds containing -CH_2-CO- structure while $C_3H_5^+$ is produced mainly by unsaturated hydrocarbons [33]. As Figure 4 shows, both intensities start with a slow, gradual increase from 200°C to ca. 400°C that resulted in a very wide, flat calculated peak in the given kinetic model. The second partial peak was similar to the corresponding peaks of the other intensity curves in the previous group. The modeling approaches outlined in Section 4.2 resulted in a narrower range of fit quality: fit_{20} was 6.1% in evaluation I and it gradually grew to 7.0% in evaluation VIII. The difference between the fit_{20} values of evaluations III and VI was only 0.08. Accordingly Evaluation VI was selected for intensities m/z 27 and m/z 41 because it expresses better the similarities than Evaluation III. In this way common $E_{0,j}$, σ_j were employed for all experimental curves and the pre-exponential factors were assumed not depending on the tobacco properties. The results are shown in Table 7 and Fig. 4.

The first pseudocomponent comprised a particularly wide range of decomposing species in all evaluations of m/z 27 and 41, as Fig. 4 illustrates and the peak width data (FWHM) indicate in Table 7. Nevertheless, the obtained $E_{0,j}$ values are close to the corresponding values of Evaluation II – VI in Table 5.

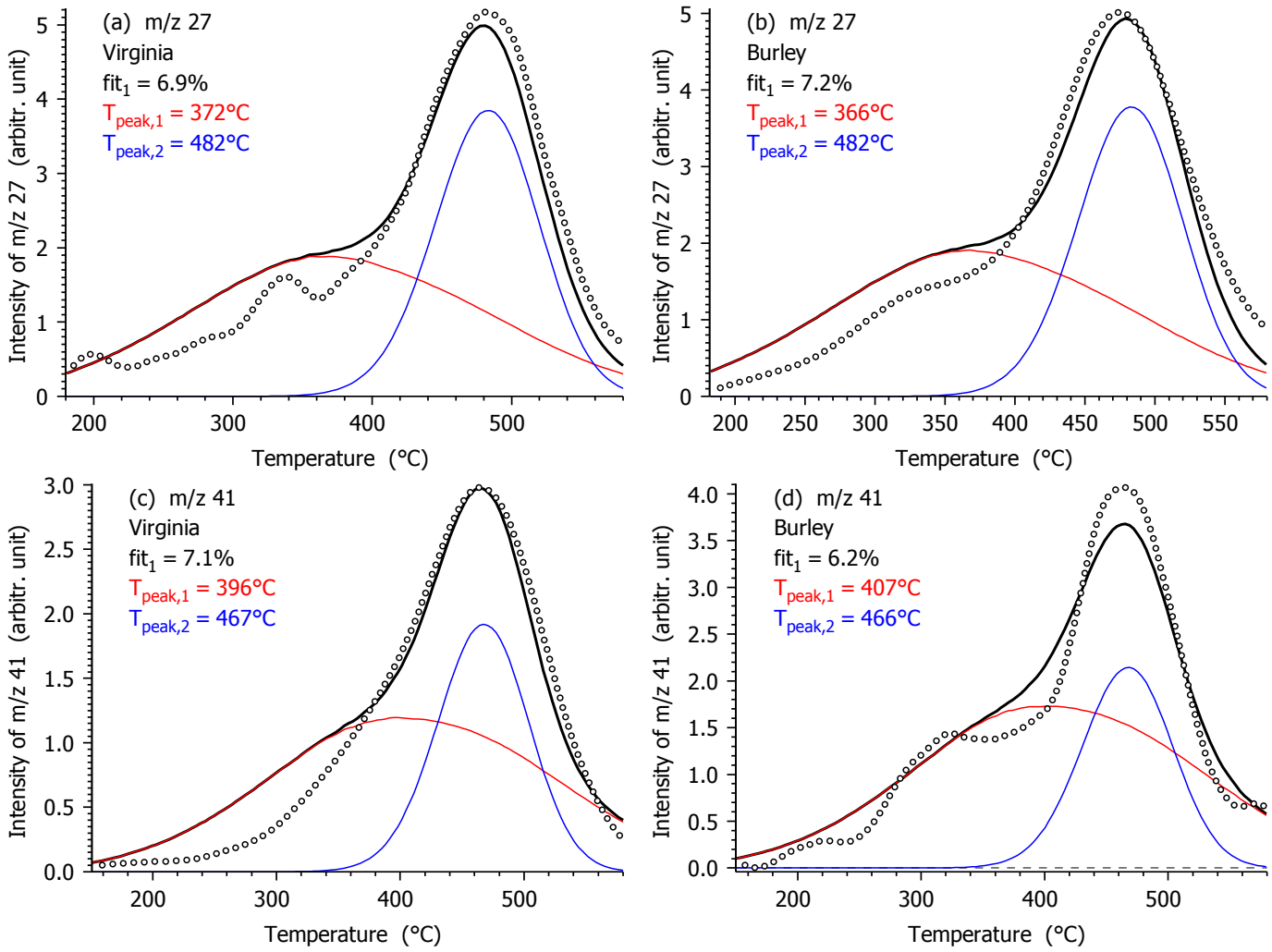

Fig. 4. Simultaneous evaluation of twenty MS intensity curves as described in Section 4.4. The experimental data (∘∘∘), their simulated counterparts (—) and the calculated partial curves (—) are shown for the 10°C/min experiments. The corresponding parameters are listed in Table 7.

Table 7
Joint evaluation of two mass spectrometric intensities by assuming common $E_{0,j}$ and σ_j values and pre-exponential factors that do not depend on the tobacco type.

MS ion	m/z 27		m/z 41	
Sample	V	B	V	B
fit_{10} / %	6.4		6.3	
$E_{0,1}$ / kJ mol^{-1}	206			
$E_{0,2}$ / kJ mol^{-1}	261			
σ_1 / kJ mol^{-1}	32.9			
σ_2 / kJ mol^{-1}	10.9			
$\log_{10} A_1$ / s^{-1}	14.29		13.47	
$\log_{10} A_2$ / s^{-1}	15.83		16.22	
$c_1 / 10^3$	2.2	2.2	1.7	2.2
$c_2 / 10^3$	1.6	1.5	0.9	0.9
$N_{parameters}$/N	1.6			
Characteristics of the calculated peaks at 10°C/min:				
$T_{peak,1}$	372	366	396	407
$T_{peak,2}$	482	482	467	466
$FWHM_1$	249	249	269	272
$FWHM_2$	89	88	88	87

4.5. Evaluation of the rest of the mass spectrometric intensities

Four of the studied mass spectrometric intensities showed markedly different behavior from those of the previous groups:

m/z 2 H_2

m/z 18 H_2O

m/z 28 mainly carbon monoxide

m/z 31 CH_3O^+ (e.g. from methanol)

These intensities were evaluated by the same strategies and assumptions as the DTG data, employing assumptions 1 – 5 of Table 4. (See Section 4.1.) In Evaluation 1 each sample was evaluated separately and the evaluation was based on five experimental curves for each intensity curve. In Evaluations 2 – 5 the 10 experiments were evaluated simultaneously for each intensity curve assuming that part of the parameters do not depend on the type of tobacco. The overall performance of an evaluation type was characterized by the corresponding fit_{40} that expresses the fit quality of the 40 experimental curves in this group. fit_{40} values of 5.5, 5.7, 6.0, 6.9 and 7.3 % were obtained for Evaluations 1 – 5, respectively. The fit_{10} values of the individual intensities also varied in this order. Similarly to Section 4.1, Evaluation 3

was selected for a detailed presentation because the corresponding fit_{10} values were not far from the fit_{10} value of the unconditional evaluation (Evaluation 1). In Evaluation 3 $E_{0,j}$ and σ_j were assumed to be independent from the tobacco type. The results are shown in Table 8 and Fig. 5.

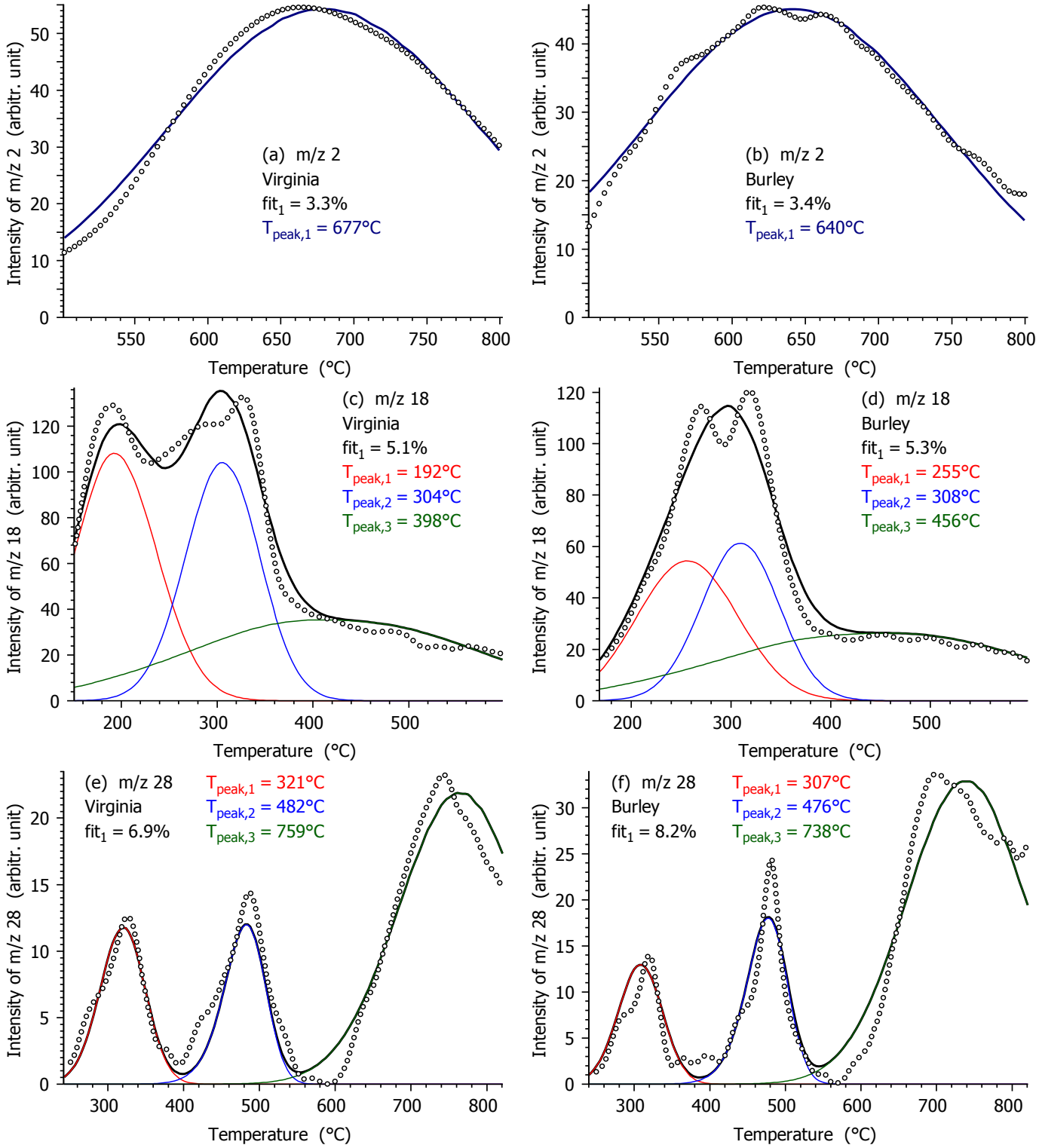

Fig. 5. Evaluation of groups of ten MS intensity curves as described in Section 4.5. The experimental data (∘∘∘), their simulated counterparts (—) and the calculated partial curves (—) are shown for the 10°C/min experiments. The corresponding parameters are listed in Table 8.

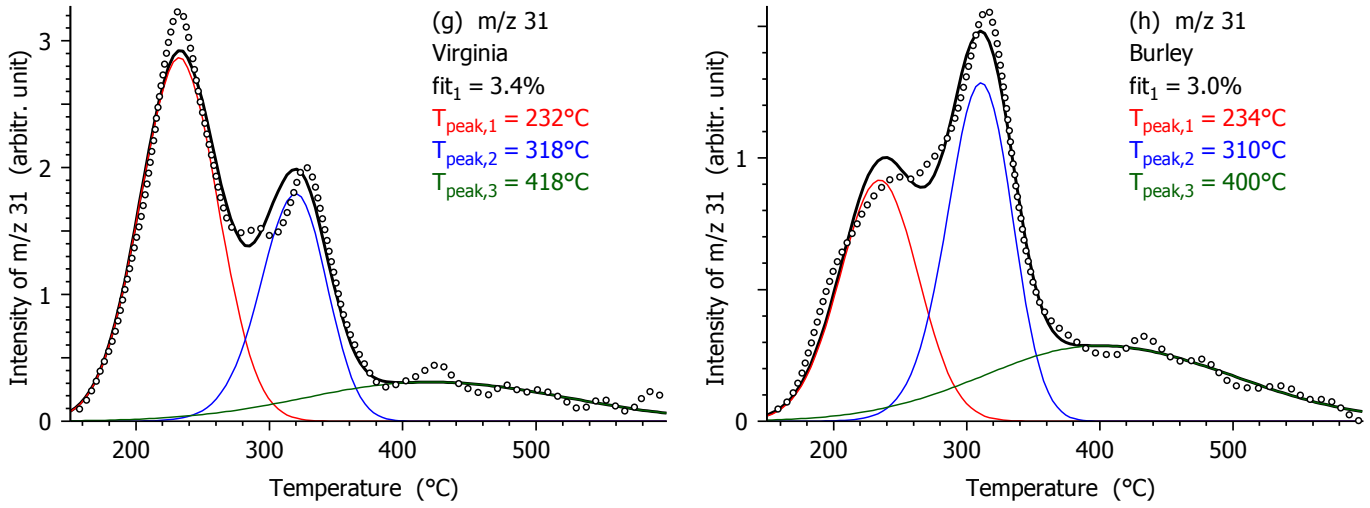

Fig. 5. *(Continued.)*

Table 8
Evaluation of mass spectrometric intensities by assuming that $E_{0,j}$ and σ_j are independent of tobacco type.

MS ion	m/z 2		m/z 18		m/z 28		m/z 31	
Sample	V	B	V	B	V	B	V	B
fit_{10} / %	5.1		5.4		8.1		4.6	
$E_{0,1}$ / kJ mol^{-1}	265		156		206		155	
$E_{0,2}$ / kJ mol^{-1}	–		177		239		184	
$E_{0,3}$ / kJ mol^{-1}	–		151		400		106	
σ_1 / kJ mol^{-1}	29.7		14.3		9.0		7.8	
σ_2 / kJ mol^{-1}	–		10.8		5.6		5.7	
σ_3 / kJ mol^{-1}	–		31.2		30.1		13.2	
$\log_{10} A_1$ / s^{-1}	12.07	12.72	15.37	13.17	16.03	16.41	13.93	13.87
$\log_{10} A_2$ / s^{-1}	–		13.82	13.71	14.36	14.48	14.07	14.32
$\log_{10} A_3$ / s^{-1}	–		8.95	8.55	17.77	18.31	5.37	5.60
$c_1 / 10^3$	68.9	55.7	55.0	39.1	5.3	4.3	1.0	0.4
$c_2 / 10^3$	–	–	49.1	35.0	5.1	5.8	0.6	0.4
$c_3 / 10^3$	–	–	64.8	59.5	26.7	29.5	0.4	0.4
$N_{parameters}$/N	1.4		2.6		2.6		2.6	
Characteristics of the calculated peaks at 10°C/min:								
$T_{peak,1}$	677	640	192	255	321	307	232	234
$T_{peak,2}$	–		304	308	482	476	318	310
$T_{peak,3}$	–		398	456	759	738	418	400
$FWHM_1$	255	243	102	120	70	69	69	68
$FWHM_2$	–		91	93	65	64	57	58
$FWHM_3$	–		355	367	191	178	227	220

The $E_{0,3}$ parameter of the m/z 28 intensity curve tended to increase to nearly 500 kJ mol^{-1}. As plots (e) and (f) of Figure 4 show, the third partial reaction of intensity m/z 28 occurred above 600°C, where no

isothermal steps was employed. (See Fig. 1. Note that 600°C was above the temperature domain of the main decomposition reactions at the heating rates of this study.) Besides, the CO evolution is not finished in the domain of investigation; the m/z 28 peaks are incomplete, as shown in Fig. 4. Accordingly this partial peak is less defined than the others from a mathematical point of view and we did not attribute a physical meaning to the obtained high $E_{0,3}$. A constraint of $E_{0,3} \leq 400$ kJ mol^{-1} was employed in this iteration. Similarly to earlier researchers [10,12] the present work also revealed a compensation effect between E_0, σ and A. In the present case an increase of $E_{0,3}$ from 400 to 450 kJ mol^{-1} improved the corresponding fit_{10} value only by 0.03, while σ_3 changed from 30.1 to 34.0 kJ mol^{-1} and A_3 increased from ca. 10^{18} to ca. 10^{21} s^{-1}. Accordingly the above mentioned $E_{0,3} \leq 400$ kJ mol^{-1} constraint is only a practical means to stop an ill-defined increase of $E_{0,3}$.

Similarly to the DTG evaluations, the widths of the simulated peaks (FWHM) showed little variation between the samples in this evaluation. Accordingly, the difference between the samples was expressed mainly by the differences in the peak temperatures and peak areas. The only exception was the first peak of the water evolution curve, where the difference between the peak width values was around 20% (18°C). In this case the peak temperature also showed a high difference, 192 vs. 255°C.

The mass spectrometric intensities of this group cover a wide variety of chemical reactions. A few aspects are listed here as follows.

(a) **m/z 2**: The hydrogen release is mainly due to the formation and carbonization of the charcoal structure, when smaller units build large, highly cross-linked structures with aromatic and π bonds. This intensity evidenced a low, flat section below ca. 500°C that was not evaluated.

(b) **m/z 18**: The low temperature water formation is due to the dehydration reactions. As Table 1 shows, the total sugar content of the Virginia and Burley tobacco blends are 13.2 and 0.1 %, respectively. Accordingly the peak around 192°C is probably due to the dehydration reactions of the sugars. Baker at al [27] showed that the first, dehydration peak of the sugars occur in a wide range: 120°C (D-fructose), 140°C (molasses), 150°C (glucose and invert sugar), 250-260°C (sucrose). The catalytic effect of minerals may complicate further the situation.

The water release between 250 and 400°C could be due mainly to the decomposition of the hemicellulose and cellulose. It was shown previously that the water release peak of cellulose can be around 310°C in a sunflower stem containing 10% ash [26]. Another sunflower stem with 4.5% ash evidenced a cellulose peak around 334°C while the reduction of the ash content by a washing process resulted in a cellulose peak of 387°C [26]. Accordingly, the partial peaks around 300°C are probably due to the decomposition of cellulose and hemicelluloses. At higher temperatures the water evolution was due to the charcoal formation. The broad, uneven water evolution signal above 600°C was not evaluated here.

(c) **m/z 28**: This mass per charge ratio corresponds mainly to CO, C_2H_4, and N_2. All the three can be expected from tobacco. Keeping in mind the high amount of oxygen containing molecules in the plant materials, m/z 28 is due mainly to CO. This is in agreement with the published yields of CO and C_2H_4 from tobacco pyrolysis [4]. (Note that the contribution of CO_2 was subtracted from this intensity, as described in the Experimental section. There are other compounds, too, that produce CO^+ fragment ions, but their combined contributions are thought to be small.)

Three peaks were observed on the intensity curve at m/z 28. The first corresponds to the pyrolysis of the thermally labile biomass components. This process starts with the decomposition of the carboxylic groups which is followed by the main decomposition step of hemicellulose and other thermally labile species.

The second peak temperature, $T_{peak,2} \approx 480$°C at 10°C/min is near to the $T_{peak,2}$ = 475 - 489°C values obtained for m/z 27, 29 and 30. (See Tables 6, 7 and 8.) The corresponding $E_{0,2}$ values in Tables 6 and 7 were 266 and 261 kJ mol^{-1}, while the $E_{0,2}$ was 239 kJ mol^{-1} in the present case. This deviation, however, is not significant due to above mentioned compensation effect between A, E_0 and σ. When the evaluation of the m/z 28 intensity was repeated at fixed $E_{0,2}$ = 266 kJ mol^{-1}, fit_{10} increased only from 8.13 to 8.15%. The change 11% of $E_{0,2}$ was compensated by a change of $A_{0,2}$ (from around 10^{14} to 10^{16} s^{-1}) and $\sigma_{0,2}$ (from 5.6 to 7.0 kJ mol^{-1}). The connection between m/z 27, 28, 29 and 30 is the contribution of the C_2 volatiles to these intensities. It is possible that the C_2 volatiles dominate in the interval of the second simulated peak of m/z 28. There is a significant difference, however between the second peak of m/z 28 and those of m/z 27, 29 and 30: the second peak of m/z 28 is relatively sharp, its $\sigma_{0,2}$ and $FWHM_2$ values are much lower than the corresponding data of the m/z 27, 29 and 30 intensities.

The reactions above 600°C were due to the slow rearrangement reactions of the char producing H_2, H_2O and CO. The decomposition of the mineral carbonates may also add to the CO evolution after a reduction of the carbonate CO_2. As the c_j values show in Table 8, the area of the third calculated peak of m/z 28 is around five times larger than those of the first and second calculated peaks.

(d) **m/z 31** is mainly due to methanol, but other oxygen containing compounds also contribute to it. For example, m/z 31 is the most abundant peak of glycolaldehyde. The peak maxima and peak width values of this intensity are nearly identical at the two samples. There are characteristic differences, however, in the area of the partial curves: c_1 and c_2 are much higher in the Virginia blend, while c_3 is nearly the same in the two samples.

5. Conclusions

The thermal decomposition of a Virginia and a Burley tobacco blend was studied by thermogravimetry – mass spectrometry at linear and stepwise heating programs. The chemical composition of the samples differed markedly. The DTG curves and 11 mass spectrometric intensities were evaluated. The

complexity of the studied materials required the use of more than one DAEM reaction. Such parameters were determined by the method of least squares that provided fits for the experiments at linear and stepwise heating programs.

The evaluated data obviously contained experimental uncertainties. Some of them are inherent in evolved gas analysis. Other uncertainties are specific to the given analysis technique. Besides, the employed model has some mathematical compensation effects as it had already been described by earlier investigators. For example, ca. 10% change in E_0 can be well compensated by a proper change of the corresponding distribution width and pre-exponential factor.

Due to these complicating factors, larger series of experiments (10 – 50 experimental curves) were evaluated simultaneously with several common parameters. In a larger series the various uncertainties can better be averaged out by the method of least squares. Besides, the number of the unknowns determined from an experiment ($N_{\text{parameters}}/N$) decreases in this way and the parameters became better determined from a mathematical point of view. In the present work $N_{\text{parameters}}/N$ varied between 1.3 and 3.2.

When ten experiments of a given curve type were evaluated together, the assumptions covered the dependence of the parameters on the tobacco properties. The first step was to assume common $E_{0,j}$ values which hardly affected the fit due to the compensation effect mentioned above. Then the number of common parameter increased till all kinetic parameters ($E_{0,j}$, A_j, and σ_j) were common and only the peak areas (c_j factors) depended on the tobacco type.

When the fifty experimental curves of five mass spectrometric intensities were evaluated together, an additional assumption became possible on the scope of the parameters: the means of the activation energy could be assumed to be the same for all the fifty curves evaluated.

The assumptions on the scope of the parameters were tested in several combinations. Some of the combinations gave better fits while others allowed the handling of five mass spectrometric intensities with the same kinetic parameters.

The approaches outlined in this work are regarded as different approximations (alternative ways of approximate modeling) of the physical reality. They are thought to be helpful in developing more realistic pyrolysis and combustion models and also in the investigation of biomass and other organic materials of complex composition by various thermal analysis techniques.

Several earlier works employed multiple DAEM reactions for the description of volatile formation in tobacco and biomass pyrolysis [2-6,9-10]. The differences of the present work from its predecessors can be summarized as follows:

a) the modeling was based on experiments with linear and stepwise temperature programs;
b) larger series of experiments were evaluated together to achieve well-defined parameter estimation;

c) various assumptions were tested to express the similarity of the experimental curves by common kinetic parameters;

d) parameters ("scale factors") were introduced to describe such issues as the slightly different dilution of the volatile products by the carrier gas at different heating programs;

e) a least squares procedure was employed that fitted high-precision simulated data to larger series of experiments.

References

[1] A.K. Burnham, R.L. Braun, Global kinetic analysis of complex materials, *Energy Fuels* 13 (1999) 1-22.

[2] E. Avni, R.W. Coughlin, P.R.Solomon, H.H. King, Mathematical modelling of lignin pyrolysis, *Fuel* 64 (1985) 1495-1501.

[3] M.A. Wójtowicz, R. Bassilakis, W.W. Smith, Y. Chen, R.M. Carangelo, Modeling the evolution of volatile species during tobacco pyrolysis, *J. Anal. Appl. Pyrolysis* 66 (2003) 235-261.

[4] S-C. Yi, M.R. Hajaligol, Product distribution from the pyrolysis modeling of tobacco particles, *J. Anal. Appl. Pyrolysis* 66 (2003) 217-234.

[5] A.A. Rostami, M.R. Hajaligol, S.E. Wrenn, A biomass pyrolysis sub-model for CFD applications, *Fuel* 83 (2004) 1519–25.

[6] S-C. Yi, M.R. Hajaligol, S.H. Jeong, The prediction of the effects of tobacco type on smoke composition from the pyrolysis modeling of tobacco shreds, *J. Anal. Appl. Pyrolysis* 74 *(*2005) 181-192.

[7] M.S. Saidi, M.R. Hajaligol, F. Rasouli, Numerical simulation of a burning cigarette during puffing, *J. Anal. Appl. Pyrolysis* 72 (2004) 141-152.

[8] R. Bassilakis, Y. Zhao, P. R. Solomon, and M. A. Serio, Sulfur and nitrogen evolution in the argonne coals: Experiment and modeling, *Energy Fuels* 7 (1993) 710-720.

[9] W. de Jong, A. Pirone, M.A. Wójtowicz, Pyrolysis of Miscanthus Giganteus and wood pellets: TG-FTIR analysis and reaction kinetics, *Fuel* 82 (2003) 1139-47.

[10] W. de Jong, G. Di Nola, B.C.H. Venneker, H. Spliethoff, M.A. Wójtowicz, TG-FTIR pyrolysis of coal and secondary biomass fuels: Determination of pyrolysis kinetic parameters for main species and NO_x precursors, *Fuel*, 86 (2007) 2367-2376.

[11] A.K. Burnham, R.L. Braun, H.R. Gregg, Comparison of methods for measuring kerogen pyrolysis rates and fitting kinetic parameters, Energy Fuels 1 (1987) 452-458.

[12] A. Holstein, R. Bassilakis, M.A. Wójtowicz, M.A. Serio, Kinetics of methane and tar evolution during coal pyrolysis, *Proc. Comb. Inst.* 30 (2005) 2177-2185.

[13] G. Várhegyi, P. Szabó, M. J. Antal, Jr., Kinetics of charcoal devolatilization, *Energy Fuels* 16 (2002) 724-731.

[14] M. Becidan, G. Várhegyi, J. E. Hustad, Ø. Skreiberg, Thermal decomposition of biomass wastes. A kinetic study, *Ind. Eng. Chem. Res.* 46 (2007) 2428 - 2437.

[15] G. Várhegyi, Aims and methods in non-isothermal reaction kinetics, *J. Anal. Appl. Pyrolysis* 79 (2007) 278-288

[16] Zs. Czégény, M. Blazsó, G. Várhegyi, E. Jakab, C. Liu, L. Nappi, Formation of selected toxicants from tobacco under different pyrolysis conditions, *J. Anal. Appl. Pyrolysis* 85 (2009) 47-53.

[17] M. Blazsó, T. Székely, F. Till, G. Várhegyi, E. Jakab, P. Szabó, Pyrolysis GC-MS and TG-MS investigation of brown coals, *J. Anal. Appl. Pyrolysis* 8 (1985) 255-269.

[18] G. Várhegyi, Kinetic evaluation of non-isothermal thermoanalytical curves in the case of independent reactions, *Thermochim. Acta* 28 (1979) 367-376.

[19] G. Várhegyi, H. Chen, S. Godoy, Thermal decomposition of wheat, oat, barley and *Brassica carinata* straws. A kinetic study, *Energy Fuels* 23 (2009) 646-652.

[20] G. Várhegyi, F. Till, Computer processing of thermogravimetric - mass spectrometric and high pressure thermogravimetric data. Part 1. Smoothing and differentiation, *Thermochim. Acta*, 329 (1999) 141-145.

[21] E. Donskoi; D.L.S. McElwain, Optimization of coal pyrolysis modeling, *Combust. Flame*, 122 (2000) 359-367.

[22] IMSL Fortran Library User's Guide, MATH/LIBRARY Volume 1, 2003, Visual Numerics Inc, Houston, Texas 77042.

[23] G. Várhegyi, Integration of the rate constant and linearization of the kinetic equations in nonisothermal reaction kinetics, *Thermochim. Acta*, 25 (1978) 201-207.

[24] T.G. Kolda, R.M. Lewis, V. Torczon, Optimization by direct search: New perspectives on some classical and modern methods, *SIAM Review* 45 (2003) 385-482.

[25] F. Shafizadeh, A.G.W. Bradbury, W.F. DeGroot, T.W. Aanerud, Role of inorganic additives in the smoldering combustion of cotton cellulose, *Ind. Eng. Chem. Prod. Res. Dev.*, 21 (1982) 97-101.

[26] G. Várhegyi, E. Jakab, F. Till, T. Székely, Thermogravimetric - mass spectrometric characterization of the thermal decomposition of sunflower stem, *Energy Fuels*, 3 (1989) 755-760.

[27] R.R. Baker, S. Coburn, Ch. Liu, J. Tetteh, Pyrolysis of saccharide tobacco ingredients: a TGA-FTIR investigation, *J. Anal. Appl. Pyrolysis* 74 (2005) 171-180.

[28] T. Fisher, M. Hajaligol, B. Waymack, D. Kellogg, Pyrolysis behavior and kinetics of biomass derived materials, *J. Anal. Appl. Pyrolysis* 62 (2002) 331-349.

[29] G. Várhegyi, M. J. Antal, Jr., E. Jakab, P. Szabó, Kinetic modeling of biomass pyrolysis, *J. Anal. Appl. Pyrolysis* 42 (1997) 73-87.

[30] E. Jakab, O. Faix, F. Till, T. Székely, Thermogravimetry/mass spectrometry study of six lignins within the scope of an international round robin test, *J. Anal. Appl. Pyrolysis* 35 (1995) 167-179.

[31] G. Várhegyi, M. J. Antal, Jr., T. Székely, F. Till, E. Jakab, Simultaneous thermogravimetric - mass spectrometric studies on the thermal decomposition of biopolymers. Part 1: Avicel cellulose in the presence and absence of catalysts, *Energy Fuels* 2 (1988) 267-272.

[32] G. Várhegyi, M. J. Antal, Jr., T. Székely, F. Till, E. Jakab, P. Szabó, Simultaneous thermogravimetric - mass spectrometric studies on the thermal decomposition of biopolymers. Part 2: Sugar cane bagasse in the presence and absence of catalysts, *Energy Fuels* 2 (1988) 273-277.

[33] F.W. McLafferty, R. Venkataraghavan, Mass Spectral Correlations. *Advances in Chemistry Series 40*, American Chemical Society, Washington, D.C., 1982.